Vacuum Packaging Technology Using Localized Aluminum/Silicon-to-Glass Bonding

Yu-T. Cheng, Wan-Tai Hsu, *Member, IEEE*, Khalil Najafi, *Fellow, IEEE*, Clark T.-C. Nguyen, *Student Member, IEEE*, and Liwei Lin

***Abstract*—A glass vacuum package based on localized aluminum/silicon-to-glass bonding has been successfully demonstrated. A constant heat flux model shows that heating can be confined locally in the dielectric layer underneath a microheater as long as the width of the microheater and the thickness of silicon substrate are much smaller than the die size and a good heat sink is placed underneath the silicon substrate. With 3.4 W heating power, $\sim$ 0.2 MPa applied contact pressure and 90 min wait time before bonding, vacuum encapsulation at 25 mtorr ($\sim$ 3.33 Pa) can be achieved. Folded-beam comb drive μ-resonators are encapsulated and used as pressure monitors. Long-term testing of vacuum-packaged μ-resonators with a Quality Factor (Q) of 2500 has demonstrated stable operation after 69 weeks. A μ-resonator with a Q factor of $\sim$ 9600 has been vacuum encapsulated and shown to be stable after 56 weeks. [686]**

***Index Terms*—Localized heating, MEMS packaging, microresonators, vacuum encapsulation, wafer level packaging.**

I. Introduction

VACUUM and hermetic encapsulation of resonant devices is required not only to protect them from damage and contamination, but also to provide a controlled low-pressure or vacuum environment for low-loss (high Q-factor) operation. Contaminants, like moisture and dust, can greatly affect the sensitivity and resolution of μ-resonant devices. For example, because the typical mass for a very high-frequency μ-resonator is about 10^{-13} kg, even small amounts of mass-loading can cause significant resonance frequency shifts and induced phase noise [1]. In addition, most micromachined resonant devices have very large surface-to-volume ratios and vibrate in a very tight space. For such devices, viscous and squeeze-film damping effects can also reduce their Q factor [2], [3].

In microelectromechanical systems (MEMS) vacuum packaging, two major approaches have been demonstrated: the integrated encapsulation approach [2]–[7] and the postprocess packaging approach [8]–[14]. A typical integrated encapsulation approach utilizes a 2 $\sim$ 3-μm thick phosphorus-doped silicon glass (PSG) or doped polysilicon layer on top of the micromachined mechanical component as a sacrificial layer, followed by the deposition of several microns thick of polysilicon or silicon nitride layer with permeable holes as a protection shell. The permeable holes provide leakage paths to buffered hydrofluoric acid (BHF) or silicon etchant for the releasing process to free mechanical microstructures. The holes are sealed by growing another low-pressure chemical vapor deposition (LPCVD) layer of polysilicon after the releasing process. Integrated encapsulation can achieve low pressure and good hermeticity in wafer level fabrication and provide low manufacturing cost. However, the lack of controllability of cavity pressure, which is determined by the deposition conditions of CVD materials during the sealing process and the high temperature of CVD deposition are limitations of this approach [6]. Furthermore, this approach is process specific and not suitable for a wide range of MEMS packaging applications. On the other hand, the postprocess packaging approach has the potential to solve these problems and is chosen as the preferred method in this work.

In the postprocess packaging approach, integrated microsystems and protection shells are fabricated on different substrates, either silicon or glass, at the same time. The two substrates are then bonded together using silicon fusion, anodic, or low temperature solder bonding to achieve the final encapsulation. Low packaging cost can be obtained due to wafer-level processing. Low bonding temperature and short process time are both desirable process parameters in device fabrication to provide low thermal stress and high throughput. However, most chemical bonding reactions require a minimum and sufficient thermal energy to overcome the reaction energy barrier, normally called the activation energy, to initiate the reaction and to form a strong bond. As a result, high bonding temperature generally results in shorter processing time to reach the same bonding quality at a lower bonding temperature. Since thermal effects to the surrounding circuitry or MEMS devices of packaged microsystems are inevitable when bonding temperature is high, localized heating has been developed to provide to alleviate these effects for bonding-based package and assembly applications [15]–[17].

In a previous paper, a novel hermetic package using localized aluminum/silicon-to-glass bonding with excellent bonding strength and durability was reported by our group [18]. This paper presents a detailed analysis of the fundamental principle of localized heating, bonding and presents a glass package used for vacuum encapsulation of surface micromachined μ-resonators. This post-process wafer-level packaging method can be applied to a variety of MEMS devices which require controllability of the cavity pressure, low-temperature processing at the wafer-level, excellent bonding strength, low fabrication cost and high reliability.

Manuscript received May 4, 2001; revised February 28, 2002. This work was supported in part by the DARPA MTO/MEMS Program under Contract F30602-97-2-0101. The work of L. Lin was supported in part by an NSF CAREER Award (ECS-0096098). Subject Editor G. Stemme.

Y.-T. Cheng, W.-T. Hsu, K. Najafi, and C. T.-C. Nguyen are with the Center for Wireless Integrated MicrosystemsDepartment of Electrical Engineering and Computer ScienceThe University of Michigan, Ann Arbor, MI 48109 USA.

L. Lin is with the Department of Mechanical Engineering, University of California at Berkeley, Berkeley, CA 94720 USA (e-mail: yuting@us.ibm.com).

Digital Object Identifier 10.1109/JMEMS.2002.802903.

II. Package Design and Fabrication

A. Thermal Analysis

The localized heating and bonding concept is utilized for bonding two substrates as shown in Fig. 1(a). Resistive heating by using microheaters on top of a device substrate is used to form a strong bond to a silicon or glass cap. According to the results of two-dimensional (2-D) heat conduction finite element analysis [16], [19], the heating region of a 5-μm-wide polysilicon microheater covered with a Pyrex glass cap at steady state can be confined locally as long as the temperature of the silicon substrate is maintained at ambient temperature.

The physics of localized heating can be understood by solving the governing heat conduction equations for a device structure without a cap. These equations are solved under a steady-state condition with constant heat flux and adiabatic boundary conditions as illustrated in Fig. 1(b). Because the width of the microheater ($2w \approx 5\ \mu$m) used in the bonding experiment is much smaller than its length ($L \approx 500\ \mu$m), the temperature distribution around the heated region can be reasonably approximated by applying a 2-D model instead of a three-dimensional (3-D) one. The governing equations and the boundary conditions are [13], [20]

$$\alpha_1\left(\frac{\partial^2 T_1}{\partial x^2}+\frac{\partial^2 T_1}{\partial y_1^2}\right)=0 \tag{1}$$

$$\alpha_{\text{eff}}\left(\frac{\partial^2 T_2}{\partial x^2}+\frac{\partial^2 T_2}{\partial y_2^2}\right)=0 \tag{2}$$

$$\begin{aligned}
\left.\frac{\partial T_1}{\partial x}\right|_{x=0}&=\left.\frac{\partial T_2}{\partial x}\right|_{x=0}=\left.\frac{\partial T_1}{\partial x}\right|_{x=\pm L_x}=\left.\frac{\partial T_2}{\partial x}\right|_{x=\pm L_x}=0\\
T_1\big|_{y_1=0}&=T_{r.t.}\\
k_1\left.\frac{\partial T_1}{\partial y_1}\right|_{y_1=d_s}&=k_{\text{eff}}\left.\frac{\partial T_2}{\partial y_2}\right|_{y_2=0}\\
T_2\big|_{y_2=0}&=T_1\big|_{y_1=d_s}\\
k_{\text{eff}}\frac{\partial T_2}{\partial y_2}&=q(-w<x<w)\\
&=0(x<-w, x>w)\\
d_{\text{eff}}&=d_o+d_n,\ k_{\text{eff}}=\frac{k_n k_o\,(d_o+d_n)}{k_o d_n+k_n d_o}
\end{aligned} \tag{3}$$

where $T_1 = T_1(x, y_1)$, $T_2 = T_2(x, y_2)$, $\alpha_1 \alpha_{\text{eff}}$, d_s, d_{eff}, k_1 and k_{eff} are the temperature, thermal diffusivity, effective thickness and thermal conductivity of silicon substrate and electrical insulation layer, $T_{r.t.}$ is the bottom temperature of the silicon substrate, q is the heat flux density at the die surface and L_x is half of the length of a die. In most MEMS, silicon dioxide and nitride are used as electrical insulators. The effective thickness and thermal conductivity of the electrical insulation layer can be calculated from (3) where d_o, d_n, k_o, and k_n are the thickness and thermal conductivity of silicon oxide and nitride, respectively. These boundary conditions are based on the following assumptions:

1) the system will be at steady state during bonding because the time needed for the whole structure to reach thermal equilibrium is only several seconds [21] (this is much shorter than the bonding time of several minutes in these experiments or hours in other tests depending on the method of heating and bonding materials);
2) the spreading of heat in polysilicon is negligible since the lateral thermal heating length in polysilicon is much smaller than the width of polysilicon [22];
3) the heat transfered from the top surface of the die to the ambient is negligible because both natural convection and radiation are much smaller than heat conduction to the substrate at moderate temperature [21], [22]; and
4) the thermal resistance of the interface between the electrical insulation layer and the silicon substrate is negligible due to the high quality of the interface between silicon oxide, silicon nitride and silicon.

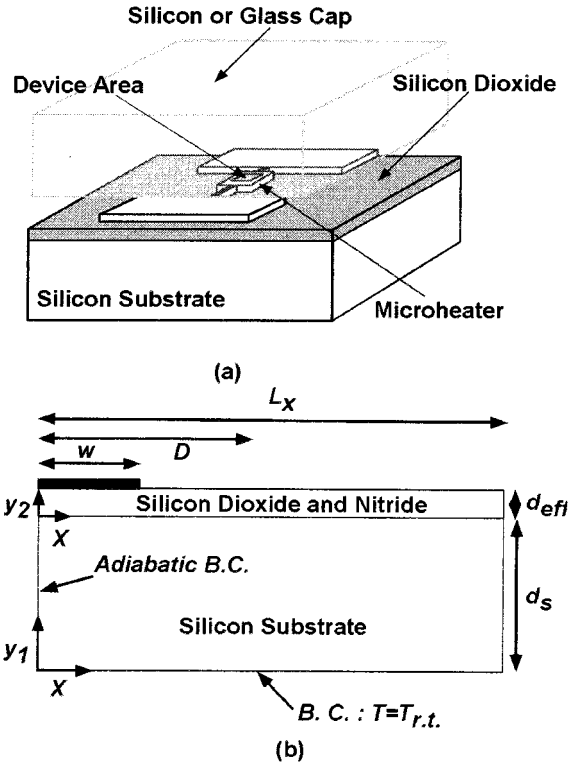

Fig. 1. Schematic diagram of localized heating and bonding. (a) 3-D view. (b) 2-D heat transfer model, geometry and boundary conditions (*B.C.*).

The analytical solutions $T_1(x, y_1)$ and $T_2(x, y_2)$ are solved as [22] (4)–(5) shown at the bottom of the next page. The temperature of the silicon substrate, T_1, is a function of thermal conductivity, heater and die size and input power. The temperature at point P, right underneath the microheater and at the interface of the electrical insulator and silicon substrate ($T_2(0,0)$, or $T_1(0, d_s)$) is

$$T_2(0,0)=T_1(0,d_s)=\sum_0^\infty B_n+T_{r.t.} \tag{6}$$

Since the thermal conductivity of silicon is about 100 times that of silicon dioxide and 50 times that of silicon nitride, the temperature of P can be approximated to the first order as:

$$\begin{aligned}
T_2(0,0)=T_1(0,d_s)&\approx\frac{q}{k_1}\left(\frac{wd_s}{L_x}\right)+T_{r.t.}\\
&\cong\frac{Q'}{k_1}\left[\frac{d_s}{L_x}\right]+T_{r.t.}
\end{aligned} \tag{7}$$

Here, Q' is the total power input per unit length into the microheater. This analysis shows the geometry of the microheater, the die size, the thermal conductivity difference between the electrical insulator and silicon and the thickness of the silicon substrate are all factors to be controlled in the bonding experiments. As long as the width of the microheater and the thickness of the silicon substrate are much smaller than the die size and a good heat sink is placed underneath the silicon substrate, heating can be confined locally. The temperature of the silicon substrate can be kept low or close to room temperature.

The bonding temperature can be estimated from the temperature of the microheater since bonding occurs at the interface between the heater and silicon or glass cap [16]. An electrothermal model of the line shaped microheater based on the law of energy conservation and the linear dependence of resistivity with respect to temperature has been developed by Lin *et al.* [21]. It has verified that it could provide a way to control bonding temperature by knowing the geometry, the input current and the temperature coefficient of resistivity of the microheater. According to this model, the total input power of the microheater is a function of the thickness of the electrical ground layer (d_{eff}) as shown in (8)–(9) at the bottom of the page where d_p, k_p, ξ_p, and F_s, are the thickness, thermal conductivity, temperature coefficient of resistivity and excess flux shape factor of the microheater, respectively and J is the input current density. Fig. 2 shows the relationship of the thickness of the silicon oxide layer and total input power density when the desired heater temperature for bonding is fixed at 800 °Cand the thickness of the silicon nitride is 0 μm in this case. It is observed that the input power density can be reduced if the thickness of the oxide layer is increased to provide better thermal isolation. On the other hand, it is also important to calculate the spreading of localized heating (by calculating D which is the distance away from the microheater where the temperature drops to 100 °C if the desired heater temperature is kept at 800 °C). This is achieved from the previous analytical solutions of the constant flux model. The surface temperature of silicon dioxide $T_2(x, d_o)$ is also a function of the oxide thickness:

$$T_2(x,d_o)=\sum_0^\infty \cos\left(\frac{n\pi}{L_x}x\right)\left[B_n\cosh(Q_n d_o)+C_n\sinh(Q_n d_o)\right]+T_{r.t.} \quad (10)$$

The simulation results show that D decreases (better for localized heating) with the decrease of oxide thickness but with the increase of the input power density as shown in Fig. 2. For example, as indicated by the arrows in the Fig. 2, D is 7.85 μm for an input power density of 1.55×10^4 Watt/cm^2 on a 5-μm-wide microheater that is on top of 7-μm-thick

$$T_1(x,y_1)=\sum_0^\infty A_n(n)\cos\left(\frac{n\pi}{L_x}x\right)\sinh(Q_n y_1)+T_{r.t.} \quad (4)$$

$$T_2(x,y_2)=\sum_0^\infty \cos\left(\frac{n\pi}{L_x}x\right)\left[B_n\cosh(Q_n y_2)+C_n\sinh(Q_n y_2)\right]+T_{r.t.} \quad (5)$$

$$A_n=\frac{qS_n}{k_{\text{eff}}Q_n\left[\sinh(Q_n d_s)\sinh(Q_n d_{\text{eff}})+\frac{k_1}{k_{\text{eff}}}\cosh(Q_n d_s)\cosh(Q_n d_{\text{eff}})\right]}$$

$$B_n=A_n\sinh(Q_n d_s)$$

$$C_n=\frac{k_1}{k_{\text{eff}}}\cosh(Q_n d_s)A_n$$

$$S_n=\frac{w}{L_x}(n=0)=\frac{2}{n\pi}\sin\left(\frac{n\pi w}{L_x}\right)$$

$$Q_n=\frac{n\pi}{L_x}$$

$$\begin{aligned}\text{Input Power}\ &=f(d_{\text{eff}})\\ &=J^2 w d_p\rho_0 L\left\{1+\xi_p\left(\frac{1}{\frac{k_{\text{eff}}F_s}{k_p d_p d_{\text{eff}}}-\frac{J^2\rho_0\xi_p}{k_p}}\left[\frac{k_{\text{eff}}F_s T_{r.t.}}{k_p d_p d_{\text{eff}}}+\frac{J^2\rho_0}{k_p}(1-\xi_p)\right]\right.\right.\\ &\quad\left.\left.-\left(\frac{1}{\frac{k_{\text{eff}}F_s}{k_p d_p d_{\text{eff}}}-\frac{J^2\rho_0\xi_p}{k_p}}\left[\frac{k_{\text{eff}}F_s T_{r.t.}}{k_p d_p d_{\text{eff}}}+\frac{J^2\rho_0}{k_p}(1-\xi_p)\right]-T_{r.t.}\right)\frac{\tanh\left(\frac{\sqrt{\varepsilon}L}{2}\right)}{\frac{\sqrt{\varepsilon}L}{2}}-T_{r.t.}\right)\right\}\end{aligned} \quad (8)$$

$$\varepsilon=\frac{k_{\text{eff}}F_s}{k_p d_p d_{\text{eff}}}-\frac{J^2\rho_0\xi_p}{k_p} \quad (9)$$

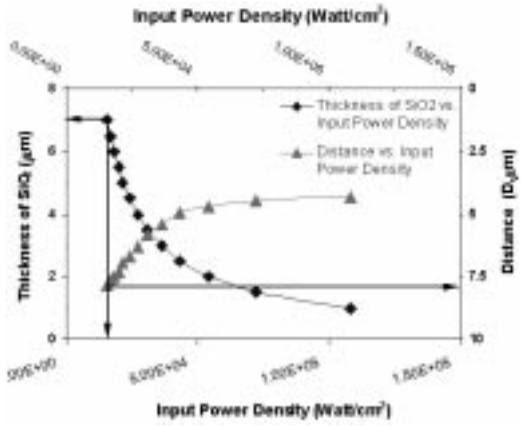

Fig. 2. Simulated results of input power density versus the thickness of silicon dioxide and the distance of the heating region where temperature is 100 °C based on a 1-D electrothermal model and a 2-D heat transfer model. The microheater is maintained at 800 °C, nitride thickness = 0 μm, $T_{rt} = 20$°C and $w = 5$ μm, in this case.

silicon oxide layer. Although reducing the oxide thickness to 1.1 μm can effectively reduce D to 4 μm, the required input power density will rise to 1.1×10^5 W/cm^2 in order to keep the microheater at 800 °C. In summary, optimized heater and insulation parameters can be determined from these analytical equations.

Because of the linear temperature dependence of polysilicon resistance, a line shaped polysilicon is used as the temperature sensor for measuring the temperature surrounding the microheater. Fig. 3 shows a polysilicon four-point resistance measurement structure as a temperature sensor 15μm away from the 5- or 7-μm-wide polysilicon microheater on top of μm thick silicon dioxide. No drastic resistivity change from the temperature sensor is measured while the microheater is heated up over 1000 °C as shown in Table I. It is estimated that every 1000 °C temperature rise in the temperature sensor corresponds to a resistivity change of up to 12%. As indicated in Table I, these results further indicate that the heating region is confined locally to within 15 μm of the heating source.

B. Vacuum Encapsulation Processes

The vacuum packaging approach presented here is based on the hermetic packaging technology using localized aluminum/silicon-to-glass solder bonding technique reported previously [18]. Built-in folded-beam comb drive μ-resonators are used to monitor the pressure inside the package. Fig. 4 shows the fabrication process of the package and resonators. Thermal oxide (2 μm) and LPCVD Si_3N_4 (3000 Å) are first deposited on a silicon substrate for electrical insulation followed by the deposition of 3000 Å LPCVD polysilicon. This polysilicon is used as both the ground plane and the electrical interconnect to the μ-resonators as shown in Fig. 4(a). Fig. 4(b) shows a 2-μm LPCVD SiO_2 layer that is deposited and patterned as a sacrificial layer for the fabrication of polysilicon μ-resonators using a standard surface micromachining process. A 2-μm-thick phosphorus-doped polysilicon is used for both the structural layer of micro resonators and the on-chip microheaters. This layer is formed over the sacrificial oxide in two steps to achieve a uniform doping profile. The resonators

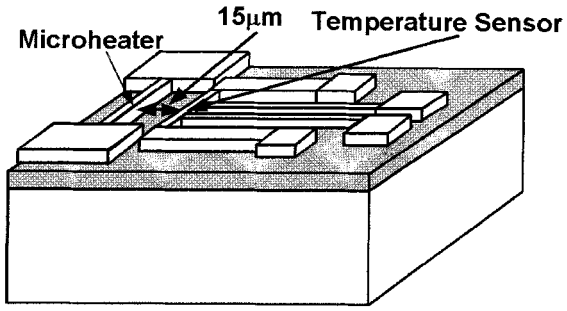

Fig. 3. Temperature measurement nearby the microheater using a polysilicon resistor.

are separated from the heater by a short distance, 30 μm, to effectively prevent their exposure to the high heater temperature as shown in Fig. 4(c).

In order to prevent the current supplied to the microheater from leaking into the aluminum solder during bonding, an LPCVD Si_3N_4 (750 Å)/SiO_2 (1000 Å)/Si_3N_4 (750 Å) sandwich layer is grown and patterned on top of the microheater as shown in Fig. 4(d). Fig. 4(e) and (f) show that polysilicon (5000 Å) and aluminum (2.5 μm) bonding materials are deposited and patterned. The sacrificial release is the final step to form free-standing μ-resonators. Fig. 4(f) shows a thick AZ-9245 photoresist is applied over the aluminum area to protect it against attack from concentrated hydrofluoric acid. After an 8-minute sacrificial release in concentrated HF, the silicon substrate as shown in Fig. 4(g) is ready for vacuum packaging. Fig. 5 shows SEM photos of a number of released μ-resonators surrounded by a 30-μm-wide microheater with aluminum/silicon bonding layer on top. A Pyrex glass cap with a 10-μm deep recess is then placed on top with an applied pressure of $\sim$ 0.2 MPa under a 25 mtorr vacuum and the heater is heated using 3.4 W input power (exact amount depends on the design of the microheaters) for 10 min to complete the vacuum packaging process as shown in Fig. 4(h).

III. Experimental Results

To evaluate the integrity of the resonators packaged using localized aluminum/silicon-to-glass solder bonding, the glass cap is forcefully broken and removed from the substrate. It is observed that no damage is found on the μ-resonator and a part of the microheater is stripped away as shown in Fig. 6, demonstrating that a strong and uniform bond can be achieved without detrimental effects on the encapsulated device. Outgassing from the glass and gas resident inside the cavity are two major factors that should be minimized in order to achieve a low pressure environment in all vacuum-based encapsulation processes.

A. Outgassing

During the bonding and encapsulation process, outgassing from the glass capsule could degrade the vacuum inside the package [23], [24]. In this encapsulation process, the volume of the cavity formed by the recessed Pyrex glass cap and the device substrate as shown in Fig. 5 is about 1.2×10^{-5} cm^3. Any outgassing would result in a drastic increase of pressure in such a small volume. Two possible outgassing mechanisms could

TABLE I
THE RESISTIVITY CHANGE OF THE POLYSILICON TEMPERATURE SENSOR

Input current, mA (5 μm wide polysilicon microheater)	0 (~25°C)*	20 (~340°C)*	30 (~1300°C)*	
Sensor resistivity (10^{-4}, Ω-cm)	9.4±0.3	9.7±0.3	9.7±0.3	
Input current, mA (7μm wide polysilicon microheater)	0 (~25°C)*	20 (~340°C)*	41 (~980°C)*	46 (~1300°C)*
Sensor resistivity (10^{-4}, Ω-cm)	9.9±0.4	9.5±0.4	9.2±0.4	9.3±0.4

*The heater temperature is estimated based on a 1-dimensional electrothermal model.

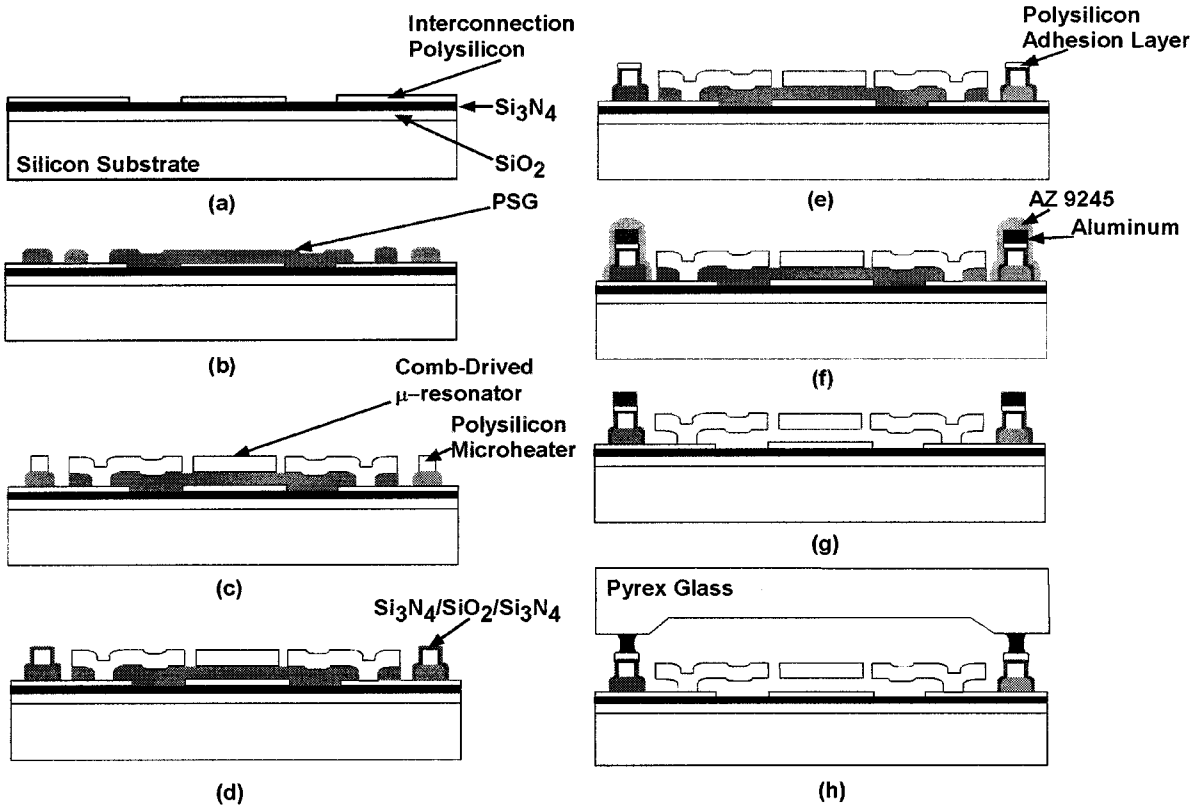

Fig. 4. Fabrication process flow of vacuum encapsulation using localized aluminum/silicon-to-glass bonding.

happen during the fabrication of vacuum packages: 1) Desorption of moisture or gases absorbed on the glass surface and 2) out-diffusion of gases which are resident in the glass. Desorption of moisture or gases can be easily eliminated by baking the glass and device substrates at a temperature above 150 °C in a vacuum oven for several hours before bonding [25]. In the case of out-diffusion of gases, the amount of gas out-diffusion is determined by the solubility difference of gases in the glass at different temperature and pressure environments. Since the glass cap is heated up during the bonding process, out-diffusion of gases from glass will occur and becomes the major factor affecting the vacuum level of the sealed cavity. For example, the solubility of helium in glass is about 6×10^{17} atoms/cm^3 at 1 atm, 300 K and will decrease to 2×10^{17} atoms/cm^3 when the temperature rises to 1000 K [26], which is about the aluminum-to-glass bonding temperature. The mean diffusion length of helium atom ($\sqrt{D_{\mathrm{He}}\, t}$, where D_{He} is the diffusion coefficient of helium in glass, $\sim$ 1000 μm^2/s at 1000 K, t is the bonding time) in Pyrex glass is about 760 μm for 10 min at 1000 K [27], which is about the thickness of the Pyrex glass cap. Therefore, if the glass cap contains the maximum amount of trapped helium and the excess helium atoms trapped inside the glass cap out-diffuse from the exposed surfaces of the cavity during the bonding process due to the outgoing gas will affect vacuum level. Theoretically, the equilibrium pressure inside the cavity at 300 K could be as high as 300 torr (40 KPa) assuming excess trapped helium gas in a volume of 500 μm $\times$ 1600 μm $\times$ 380 μm of glass is fully out-diffused and stays inside the cavity (500 μm $\times$ 1600 μm $\times$ 14 μm), even though bonding is performed in a 25 mtorr vacuum environment. In addition to helium, other gases like argon, oxygen, nitrogen could also diffuse into the cavity and increase the cavity pressure.

A two-step pretreatment of Pyrex glass can reduce the influence of gas out-diffusion. A recessed glass cap is first baked under 25 mtorr and 300 °C for 1 h and is then coated with 3000 Å Ti/1000 Å Au layers on the recessed surface. Vacuum baking can reduce the total amount of gases trapped inside the glass and metal coating can provide a good diffusion barrier to gas atoms. Furthermore, titanium is a good getter material for

Fig. 5. SEM photographs of folded-beam μ-resonators surrounded by a microheater with aluminum/silicon bonding layer on top.

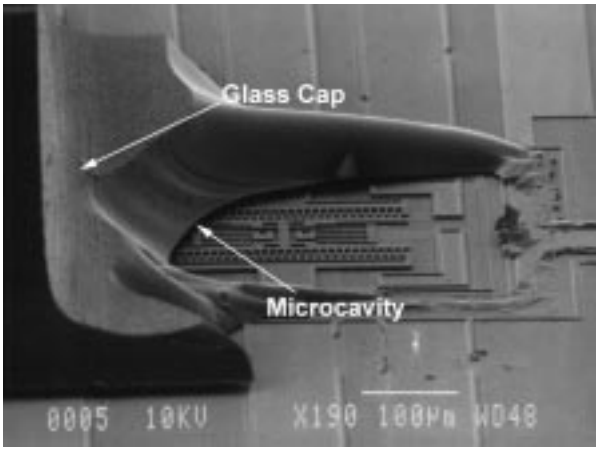

Fig. 6. The SEM photograph of encapsulated μ-resonators after the glass cap is forcefully broken away.

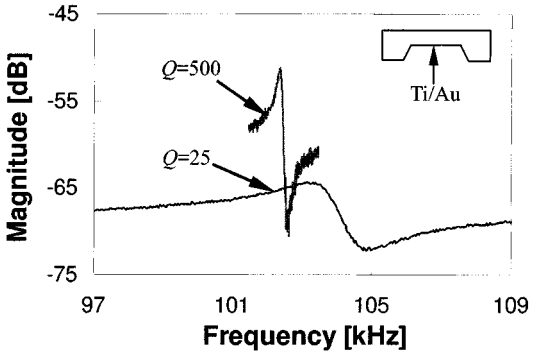

Fig. 7. Measured Q of glass encapsulated μ-resonators. The Q of a μ-resonator encapsulated using a vacuum baked and Ti/Au coated glass cap can be improved to 500.

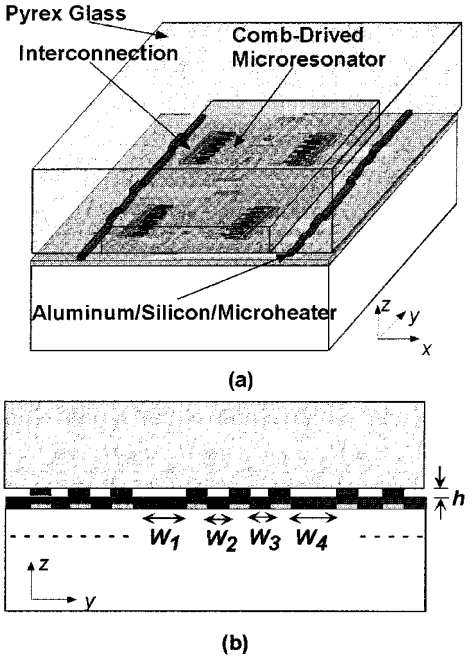

Fig. 8. The schematic diagram of packaging system. (a) 3-D view and (b) cross-sectional view. The air can leak out along the free open between glass cap and device substrate during pump down.

common gases and will further reduce the amount of trapped gases inside the package and out-gassing during the bonding process. Fig. 7 shows the Q value of μ-resonators ($\sim$ 103 kHz resonant frequency) encapsulated by glass caps with or without pretreatment and with a Ti/Au layer on the recessed surface of glass. Since the Ti/Au layer effectively prevents out-gassing from the glass cap during bonding, a quality factor improvement from 25 to 500 is observed.

B. Gas Resident Time

In the final vacuum encapsulation step, the whole packaging system is placed inside a vacuum chamber and the aluminum/silicon solder is heated up locally to initiate bonding. Since the air trapped inside the cavity has to diffuse out, it takes time for the micro-cavity to reach the same vacuum level as the outside environment in the vacuum chamber. Gas resident time is an important experimental parameter and determines when the bonding process should start after the system is placed into the chamber; it can be estimated by using fluid mechanic theory. In the current set-up, air can leak out along the open space between the glass cap and the device substrate. This can be treated as air flow between two parallel plates from the cavity to the chamber as shown in Fig. 8. The distance (h) between the two parallel plates is the same as the step height created by electrical interconnection lines which is about 3000 Å. The length of the plate, L_p, is about 100 μm and the total effective width (w_{eff} = the total sum of w_i, $i = 1, 2, 3, \ldots$) is about 1.9 mm. The laminar flow solution of the flow rate, S, along two parallel plates is [27]:

$$S = -\frac{\Delta P w_{\text{eff}} h^3}{12\mu L_p} = -\frac{w_{\text{eff}} h^3}{12\mu L_p}(P - P_{envi.}) = A(P - P_{envi.}) \quad (11)$$

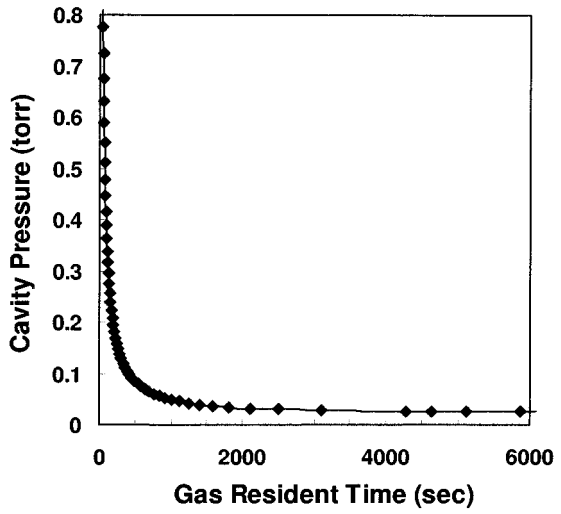

Fig. 9. Calculated cavity pressure versus the gas resident time inside the cavity (1 torr $=$ 133.3 Pa).

where μ is the viscosity of air ($\sim$ 0.018 mNsec/m^2 at 300 K), P is the cavity pressure and P_{envi}. is the chamber pressure. Based on the mass conservation law, a differential relationship between the pressure and time is derived:

$$-V\frac{dP}{dt} = S * P = A(P - P_{envi}) * P \tag{12}$$

where V represents the volume of the cavity. After rearranging and integrating this differential equation, the gas resident time can be calculated in terms of the cavity volume, the physical properties of air, the geometry of the leakage path and the pressures of the cavity and the chamber:

$$\tau = \frac{-V}{AP_{envi.}} \ln\left(\frac{P - P_{envi.}}{P}\right). \tag{13}$$

Fig. 9 shows the calculated results of the residual pressure of the cavity versus gas resident time. The cavity pressure can reach a pressure below 30 mtorr after inserting the system into a 25-mtorr vacuum chamber for about 90 min. Therefore, the Q factor can be increased by keeping the package under vacuum for an extended period of time ($>$ 10 min) before the cap is bonded to the substrate. Fig. 10 shows a μ-resonator ($\sim$ 81 kHz) with a Q factor of $\sim$ 2500 bonded at 25 mtorr after $\sim$ 90 min of pumping down.

IV. Discussion

The post-process packaging using localized heating and bonding technique includes four basic components:

1) an electrical and thermal insulation layer such as silicon dioxide or silicon nitride used for localized heating;
2) resistive microheaters needed to provide the heating source for localized bonding;
3) materials, including metal and polysilicon, which can provide good bonding and hermeticity with silicon or glass substrates; and
4) a good heat sink under the device substrate for localized heating. The process can be either die level or wafer level.

An approach to a wafer level packaging process is illustrated in Fig. 11. The resistive microheaters are connected in parallel to

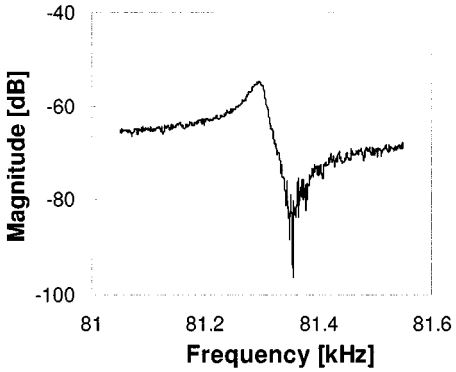

Fig. 10. The transmission spectrum of a glass-encapsulated μ-resonator with 90 min pump down time in vacuum environment ($Q = 2500$).

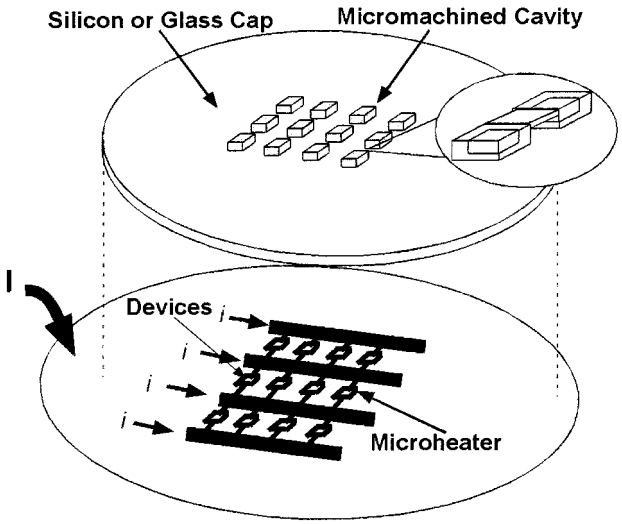

Fig. 11. Illustration of wafer-level vacuum packaging in the wafer level using localized heating and bonding technique.

achieve uniform current distribution to all heaters. Interconnects to these microheaters can be formed in the dicing lines so no extra space is required. These heaters can be either fabricated on the device substrate or the protection cap. In the case shown in Fig. 11, the microheaters are fabricated on the device substrate. In the cap substrate, the area between individual caps is partially diced before bonding. Once the bonding step is completed, the remaining material is sawed away and the device substrate is then diced. The main challenge of this wafer-level packaging approach is creating a good heat sink which could maintain a low temperature at the bottom of the device substrate since the total power consumption of localized heating could be high.

The Q factors of un-packaged resonators as a function of pressure are measured as shown in Fig. 12. It is observed that a quality factor of 2300 of a comb resonator corresponds to a vacuum level of about 25 mtorr. This result is consistent with the data shown in Fig. 10 where the pressure in the package after bonding is approximately 25 mtorr. Furthermore, the un-packaged resonators have a maximum Q of about 3850 at a very low pressure of 1 mtorr and can be improved to higher than 8000 by means of localized annealing [28]. Therefore, the lower than expected Q factor of the vacuum encapsulated resonator is not believed to be due to air damping. More testing on the

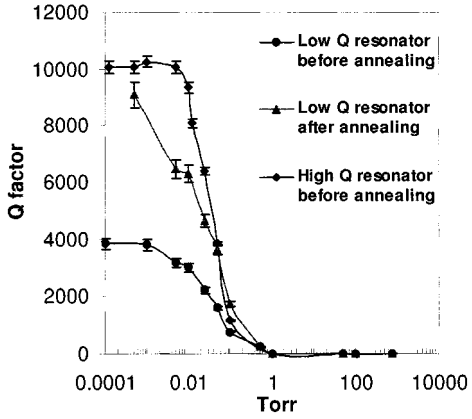

Fig. 12. Measured Q factor versus pressure of unpackaged μ-resonators.

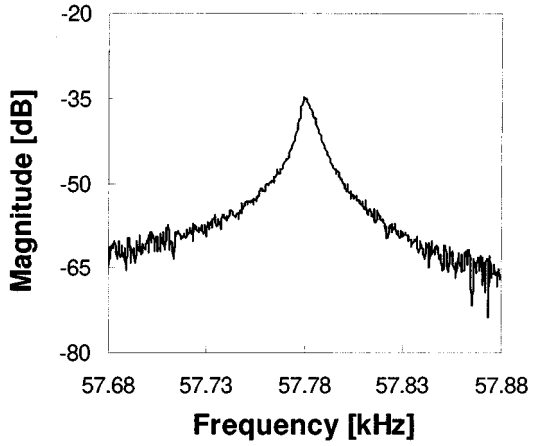

Fig. 13. The transmission spectrum of a glass-encapsulated μ-resonator after 120 min pump down time in vacuum environment ($Q = 9600$).

resonators with higher Q factor was conducted to verify this. Fig. 13 shows a vacuum encapsulated un-annealed μ-resonator ($\sim$ 57 kHz) after 120 min of pump down time. The measured Q-factor after packaging is 9600. Based on the measurement of Q versus pressure, it is demonstrated that the pressure inside the package is comparable to the vacuum level of the packaging chamber which is 25 mtorr.

At 300K and 1 atm, the mean free path of air is about 700 Å. The Knudsen number is less than 1 since the space (h) and width (w) of two parallel plates in this packaging system are larger than the mean free path. Thus, it is adequate to use laminar flow to predict the gas resident time if the chamber pressure is 1 atm. However, the mean free path of air is a function of chamber pressure. Air can have larger mean free path when the environmental pressure is low. When the cavity pressure is below 10 torr, the Knudsen Number will be close to 1 which indicates gas flow will start transitioning from viscous flow to molecular diffusion and the gas resident time will be underestimated by using the laminar flow equation. Therefore, the 10 min of pump down time before bonding is not enough. This explains the reason why the Q factor is only 500 in Fig. 7 when a pump down time of 10 min is used.

Fig. 14 shows long-term measurement of the Q factor of two un-annealed, vacuum packaged μ-resonators. It is found that both vacuum packages provide stable vacuum environments for

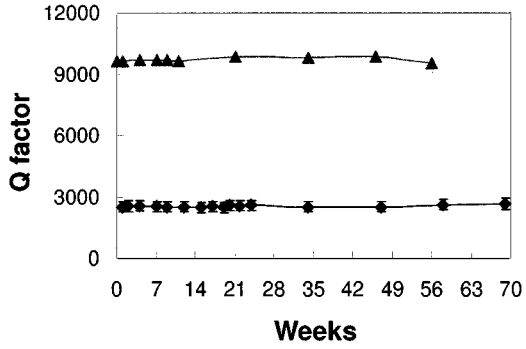

Fig. 14. Long-term measurement of encapsulated μ-resonators. No degradation of Q factors is found after 69 weeks and 56 weeks.

μ-resonators with Q factors of 2500 and 9600, respectively. No degradation of Q factors is found after 69 and 56 weeks in either package. Note that these packages have been kept at room temperature throughout this test. Tests are still continuing. Since the Q factor of a μ-resonator is very sensitive to pressure these tests indicate the pressure in the package is quite stable.

V. Conclusion

The technique of localized bonding provides several advantages over conventional MEMS packaging approaches, including the possibility of post-process packaging, no CMP (chemical-mechanical polishing) planarization process, short bonding time (about 5 $\sim$ 10 min), small bonding pressure ($<$ 1 MPa), strong chemical bond, metal alloy sealing for vacuum encapsulation, die and wafer-level bonding and self-aligned processing. Microresonators have been successfully encapsulated in vacuum based on localized aluminum/silicon-to-glass bonding. With 3.4 W of heating power, $\sim$ 0.2 MPa applied contact pressure and 90 min of pump down time in 25 mtorr of vacuum before bonding, vacuum encapsulation can be achieved. The effects of outgassing and gas resident time on the sealed micro cavity have been discussed. The use of a metal coating as a diffusion barrier as well as a wait period before bonding to achieve high vacuum inside the package are proposed. This micropackaging method provides several features, including control over the cavity pressure, low temperature processing at the wafer-level, excellent bonding strength, low fabrication cost and high reliability.

Acknowledgment

The authors would like to thank Dr. Y.-H. Me for continuing the Q factor measurement of the vacuum packaged resonators.

References

[1] C. T.-C. Nguyen and R. T. Howe, "Design and performance of monolithic CMOS micromechanical resonator oscillators," in *Proc., 1994 IEEE Int. Frequency Control Symposium*, Boston, MA, 1994, pp. 127–134.

[2] R. Legtenberg and H. A. C. Tilmans, "Electrically driven vacuum-encapsulated polysilicon resonators, Part I: Design and fabrication," *Sens. Actuators*, vol. A45, pp. 57–66, 1994.

[3] K. Ikeda, H. Kuwayama, T. Kobayashi, T. watanabe, T. Nishikawa, T. Oshida, and K. Harada, "Three-dimensional micromachining of silicon pressure sensor integrating resonant strain gauge on diaphragm," *Sens. Actuators*, vol. A21–23, pp. 1001–1010, 1990.

[4] H. Guckel, "Surface micromachined pressure transducers," *Sens. Actuators*, vol. A28, pp. 133–146, 1991.
[5] P. K. Klhanna, S. K. Bhatnagar, and W. Gust, "Analysis of packaging and sealing techniques for microelectronic modules and recent advances," *Microelectron. Int.*, vol. 16, pp. 8–12, 1999.
[6] L. Lin, R. T. Howe, and A. P. Pisano, "Microelectromechanical filters for signal processing," *J. Microelectromech. Syst.*, vol. 7, pp. 286–294, Sept. 1998.
[7] M. B. Cohn, Y. Lang, R. T. Howe, and A. P. Pisano, "Wafer-to wafer transfer of microstructures for vacuum package," in *Proc. Solid-State Sensors and Actuators Workshop*, Hilton Head, SC, June 1996, pp. 32–35.
[8] L. Parameswaran, V. M. McNeil, M. A. Huff, and M. A. Schmidt, "Sealed-cavity microstructure using wafer bonding technology," in *Proc. 7th International Conference on Solid State Sensors and Actuators, Transducers' 93*, Yokohoma, Japan, 1993, pp. 274–277.
[9] M. Bartek, J. A. Foerster, and R. F. Wolffenbuttel, "Vacuum sealing of microcavities using metal evaporation," *Sens. Actuators*, vol. A 61, pp. 364–368, 1997.
[10] D. Ando, K. Oishi, T. Nakamura, and S. Umeda, "Glass direct bonding technology for hermetic seal packaging," in *Proc. IEEE, MEMS 97*, Nagoya, Japan, 1997, pp. 186–190.
[11] H. A. C. Tilmans, M. D. J. van der Peer, and E. Beyne, "The indent reflow sealing (IRS) technique—A method for the fabrication of sealed cavities for MEMS devices," *J. Microelectromech. Syst.*, vol. 9, pp. 206–217, June 2000.
[12] D. R. Spark, L. Jordan, and J. H. Franzee, "Flexible vacuum-package method for resonating micromachines," *Sens. Actuators*, vol. A 55, pp. 179–183, 1996.
[13] K. Minami, T. Moriuchi, and M. Esashi, "Cavity pressure control for critical damping of packaged micro mechanical devices," in *Proc. 8th International Conference on Solid State Sensors and Actuators, Transducers' 95*, Stockholm, Sweden, 1995, pp. 240–243.
[14] T. Fujita, K. Hatano, T. Matsuoka, T. Kojima, T. Oshima, K. Maenaka, and M. Maeda, "Vacuum sealed silicon bulk micromachined gyroscopes," in *Proc. 10th International Conference on Solid State Sensors and Actuators, Transducers' 99*, Sendai, Japan, 1999, pp. 914–917.
[15] L. Lin, Y. T. Cheng, and K. Najafi, "Formation of silicon-gold eutectic bond using localized heating method," *Jpn. J. Appl. Phys.*, pt. II, vol. 11B, pp. 1412–1414, November 1998.
[16] Y. T. Cheng, L. Lin, and K. Najafi, "Localized silicon fusion and eutectic bonding for MEMS fabrication and packaging," *J. Microelectromech. Syst.*, vol. 9, pp. 3–8, Mar. 2000.
[17] L. Lin, "MEMS post-packaging by localized heating and bonding," *IEEE Trans. Adv. Packag.*, vol. 23, pp. 608–616, Nov. 2000.
[18] Y. T. Cheng, L. Lin, and K. Najafi, "Fabrication and hermeticity testing of a glass-silicon packaging formed using localized aluminum/silicon-to-glass bonding," in *Proc. IEEE MEMS Conf.*, 2000, pp. 757–762.
[19] ——, "A hermetic glass-silicon package formed using localized aluminum/silicon-to-glass bonding," *J. Microelectromech. Syst.*, vol. 10, pp. 392–392, Sept. 2001.
[20] F. P. Incropera and D. P. Dewitt, *Introduction to Heat Transfer*, 3rd ed. New York: Wiley, 1996, pp. 161–211.
[21] L. Lin, A. P. Pisano, and V. P. Carey, "Thermal bubble formation on polysilicon micro resistors," *J. Heat Transfer*, vol. 120, pp. 735–742, 1998.
[22] K. Kurabayashi and K. E. Goodson, "Precision measurement and mapping of die-attach thermal resistance," *IEEE Trans. Comp. Packag. Manufact. Technol., A*, vol. 21, pp. 506–514, 1998.
[23] S. Mack, H. Baumann, and U. Gösele, "Gas tightness of cavities sealed by wafer bonding," in *Proce. IEEE MEMS Conf.*, 1997, pp. 488–491.
[24] H. Henmi, S. Shoji, Y. Shoji, K. Yosimi, and M. Esashi, "Vacuum package for microresonators by glass-silicon anodic bonding," in *Proc. 7th International Conference on Solid State Sensors and Actuators, Transducers' 93*, 1993, pp. 584–587.
[25] H. A. Steinherz, *Handbook of High Vacuum Engineering*. New York: Reinhold, 1963, pp. 193–200.
[26] J. F. Shackelford, "Gas solubility in glasses-principles and structural implications," *J. Non-Crystal. Solid.*, vol. 253, pp. 231–241, 1999.
[27] R. Darby, *Chemical Engineering Fluid Mechanics*. New York: Marcel Dekker, 1996, pp. 184–193.
[28] K. Wang, A.-C. Wong, W. T. Hsu, and C.-T. C. Nguyen, "Frequency-trimming and Q factor enhancement of mi-cromechanical resonators via localized filament annealing," in *Proc. 9th International Conference on Solid State Sensors and Actuators Transducers 97*, June 16–19, 1997, pp. 109–112.

Yu-Ting Cheng was born in Taiwan, Republic of China. He received the B.S. and M.S. degrees in materials science and engineering from the National Tsing Hua University, Hsinchu, Taiwan, in 1991 and 1993, respectively, the M.S. degree in the field at Carnegie Mellon University, Pittsburgh, PA, in 1996, and the Ph.D. degree in electrical engineering at the University of Michigan, Ann Arbor, in 2000. His thesis was the development of a novel vacuum packaging technique for MEMS applications.

His research interests include the fundamental study of materials for MEMS applications, micropackaging and new hybrid micromachining fabrication of microstructures, microsensors, and microactuators. Now he is currently working for IBM Watson Research Center, Yorktown Heights, as a research staff member and involving in several SOP (System on Packaging) projects.

Dr. Cheng is a Member of Phi Tau Phi.

Wan-Thai Hsu (M'01) was born in Taipei, Taiwan, in 1968. He received the B.S. and the M.S. degrees from National Tsing-Hua University, Hsin-Chu, Taiwan, in 1990 and 1992, respectively, and the Ph.D. degree from University of Michigan, Ann Arbor, all in electrical engineering.

He was working on high-speed, self-aligned gate GaAs MESFET fabrication and testing for his M.S. degree. From 1992 to 1994, he served as a 2nd lieutenant in anti-aircraft artillery division, Taiwan air force. From 1994–1995, he was a research staff in National Tsing-Hua University, where he worked to develop a CH_4 gas sensor for environmental monitoring applications. He entered the University of Michigan in 1995 to pursue his Ph.D., where he first managed to set up a micromechanical resonator testing lab for his group, then he had been working on projects related to design, fabrication, packaging and testing for micromechanical resonators for communication applications, mainly focusing on temperature insensitive designs.

Currently, he is employed at Discera, Inc., Ann Arbor, MI, developing high-Q , high-frequency MEMS-based oscillators and filter banks. He is also actively involved in vacuum packaging and integration technologies. His research interests include: micromechanical systems, new materials for MEMS, integrated circuit design and technologies, communication architectures, merged circuit/MEMS integration/vacuum packaging technologies.

Khalil Najafi (S'84–M'86–SM'97–F'00) was born in 1958. He received the B.S., M.S., and Ph.D. degrees in 1980, 1981, and 1986 respectively, all in electrical engineering from the Department of Electrical Engineering and Computer Science, University of Michigan, Ann Arbor.

From 1986 to 1988, he was employed as a Research Fellow, from 1988 to 1990 as an Assistant Research Scientist, from 1990 to 1993 as an Assistant Professor, from 1993 to 1998 as an Associate Professor, and since September 1998 as a Professor and the Director of the Solid-State Electronics Laboratory, Department of Electrical Engineering and Computer Science, University of Michigan. His research interests include: micromachining technologies, solid-state micromachined sensors, actuators and MEMS; analog integrated circuits; implantable biomedical microsystems; hermetic micropackaging; and low-power wireless sensing/actuating systems.

Dr. Najafi was awarded a National Science Foundation Young Investigator Award from 1992 to 1997, was the recipient of the Beatrice Winner Award for Editorial Excellence at the 1986 International Solid-State Circuits Conference, of the Paul Rappaport Award for co-authoring the Best Paper published in the IEEE Transactions on Electron Devices and of the Best Paper Award at ISSCC 1999. In 1994 he received the University of Michigan's "Henry Russel Award" for outstanding achievement and scholarship and was selected as the "Professor of the Year" in 1993. In 1998, he was named the Arthur F. Thurnau Professor for outstanding contributions to teaching and research and received the College of Engineering's Research Excellence Award. He has been active in the field of solid-state sensors and actuators for more than eighteen years and has been involved in several conferences and workshops dealing with solid-state sensors and actuators, including the International Conference on Solid-State Sensors and Actuators, the Hilton-Head Solid-State Sensors and Actuators Workshop and the IEEE/ASME Microelectromechanical Systems (MEMS) Workshop.

Dr. Najafi is the Editor for Solid-State Sensors for IEEE TRANSACTIONS ON ELECTRON DEVICES, Associate Editor for IEEE JOURNAL OF SOLID-STATE CIRCUITS and an Associate Editor for the *Journal of Micromechanics and Microengineering*, Institute of Physics Publishing.

Clark T.-C. Nguyen (S'90–M'93–S'01) received the B.S., M.S., and Ph.D. degrees from the University of California at Berkeley, in 1989, 1991, and 1994, respectively, all in electrical engineering and computer sciences

In 1995, he joined the faculty of the University of Michigan, Ann Arbor, where he is presently an Associate Professor in the Department of Electrical Engineering and Computer Science. From 1995 to 1997, he was a member of the National Aeronautics and Space Administration's (NASA) New Millennium Integrated Product Development Team on Communications, which road-mapped future communications technologies for NASA use into the turn of the century. His research interests focus upon micro electromechanical systems (MEMS), including integrated micromechanical signal processors and sensors, merged circuit/micromechanical technologies, RF communication architectures and integrated circuit design and technology.

Prof. Nguyen received the 1938 E Award for Research and Teaching Excellence from the University of Michigan in 1998, an EECS Departmental Achievement Award in 1999, the Ruth and Joel Spira Award for Outstanding Teaching in 2000 and the University of Michigan's Henry Russell Award in 2001. Together with his students, he received the Roger A. Haken Best Student Paper Award at the 1998 IEEE International Electron Devices Meeting. In 1999, he Co-Chaired the Workshop on Microelectromechanical Devices for RF Systems at the 1999 IEEE MTT-S Symposium.

Liwei Lin received the M.S. and Ph.D. degrees in mechanical engineering from the University of California, Berkeley, in 1991 and 1993, respectively.

From 1993 to 1994, he was with BEI Electronics, Inc., in research and development of microsensors. From 1994 to 1996, he was an Associate Professor in the Institute of Applied Mechanics, National Taiwan University, Taiwan. From 1996 to 1999, he was an Assistant Professor at the Mechanical Engineering and Applied Mechanics Department at the University of Michigan. He joined the University of California at Berkeley in 1999 and is now an Associate Professor at Mechanical Engineering Department and Co-Director at Berkeley Sensor and Actuator Center, NSF/Industry/University research cooperative center. His research interests are in design, modeling and fabrication of microstructures, microsensors and microactuators as well as mechanical issues in microelectromechanical systems including heat transfer, solid/fluid mechanics and dynamics. He holds seven U.S. patents in the area of MEMS.

Dr. Lin is the recipient of the 1998 NSF CAREER Award for research in MEMS Packaging and the 1999 *ASME Journal of Heat Transfer* Best Paper Award for his work on microscale bubble formation. He led the effort in establishing the MEMS subdivision in ASME and is currently serving as the Vice Chairman of the Executive Committee for the MEMS subdivision.